Dynamics of Atmospheres and Oceans 48 (2009) 121–142

Contents lists available at ScienceDirect

Dynamics of Atmospheres and Oceans

journal homepage: www.elsevier.com/locate/dynatmoce

A comparison of shelf observation platforms for assimilation in an eddy-resolving ocean model

Peter R. Oke[a,b,*], Pavel Sakov[a,b,c], Eric Schulz[a]

[a] *Centre for Australian Weather and Climate Research: A Partnership between CSIRO and the Bureau of Meteorology, Hobart, Tasmania, Australia*
[b] *Wealth from Oceans National Research Flagship, Australia*
[c] *Nansen Environmental and Remote Sensing Center, Bergen, Norway*

ARTICLE INFO

Article history:
Available online 3 May 2009

Keywords:
Data assimilation
Coastal observing systems

ABSTRACT

An assessment of the likely benefits of assimilating in situ temperature (T) and salinity (S) observations from repeat glider transects and surface velocity observations from high-frequency radar arrays into an eddy-resolving ocean model is presented. The deployment of new shelf observation platforms around Australia is being undertaken through the Australian Integrated Marine Observing System program. In this study, various options for an observing system along the coast of New South Wales, Australia, are assessed for their benefits to an ocean forecast and reanalysis system. The forecast system considered here uses ensemble optimal interpolation (EnOI) for data assimilation. Using error estimates from the EnOI scheme, estimates of the theoretical analysis errors are calculated for different observing systems that include a range of remotely sensed and in situ observations. The results demonstrate that if HF radar observations are assimilated along with the standard components of the global ocean observing system, the analysis errors are likely to reduce by as much as 80% for velocity and 60% for T, S and sea-level in the vicinity of the observations. Owing to the relatively short along-shore decorrelation length-scales for T and S near the shelf, the glider observations are likely to provide the forecast system with a more modest gain.

* Corresponding author at: CSIRO Marine and Atmospheric Research, Castray Esplanade, GPO Box 1538, Hobart 7001, Tasmania, Australia. Tel.: +61 362325387; fax: +61 362325123.
E-mail addresses: peter.oke@csiro.au (P.R. Oke), pavel.sakov@nersc.no (P. Sakov), E.Schulz@bom.gov.au (E. Schulz).
URL: http://www.cmar.csiro.au/staff/oke/ (P.R. Oke).

0377-0265/$ – see front matter © 2009 Elsevier B.V. All rights reserved.
doi:10.1016/j.dynatmoce.2009.04.002

1. Introduction

This study is motivated by the expanding shelf observational capabilities introduced under the Australian Integrated Marine Observing System (IMOS) program (www.imos.org.au). Briefly, IMOS involves the provision of observational platforms (e.g., gliders, high-frequency radars, moorings) to establish a long-term monitoring capability for the oceans around Australia. These observations can be readily assimilated into both ocean reanalyses and ocean forecast systems.

In response to the IMOS program we seek to assess the likely improvements to ocean forecasts and reanalyses by assimilating observations from different shelf observation platforms into an eddy-resolving ocean model. In addition, we seek to demonstrate how an ensemble-based data assimilation system can be used to aid the design of observation networks. The methods used here are simple and computationally efficient and help build intuition about the likely scales, processes and dynamics that are represented by different observation types.

The ocean reanalysis and forecast system considered here was developed under the Bluelink project (www.bom.gov.au/bluelink/). The primary objective of Bluelink is the development of a forecast system for the mesoscale ocean circulation in the Australian region. The Bluelink forecast system became operational at the Bureau of Meteorology in August 2007 (www.bom.gov.au/oceanography/forecasts/). The main components of the Bluelink system are the Ocean Forecasting Australia Model (OFAM; Schiller et al., 2008) and the Bluelink Ocean Data Assimilation System (BODAS; Oke et al., 2005, 2008). The primary testbed for the Bluelink system is the Bluelink ReANalysis (BRAN), a multi-year integration of OFAM that assimilates observations sequentially using BODAS.

One of the most challenging and interesting regions around Australia to reanalyse and forecast is the Tasman Sea off the New South Wales (NSW) coast. The circulation in this region includes variability of the East Australian Current (EAC) and a complex mesoscale eddy field (Fig. 1). The spatial scales in the EAC eddy field can be quite short, often with small, but energetic cold-core eddies. These types of oceanic features are at the observational limits of the global ocean observing system (GOOS). This

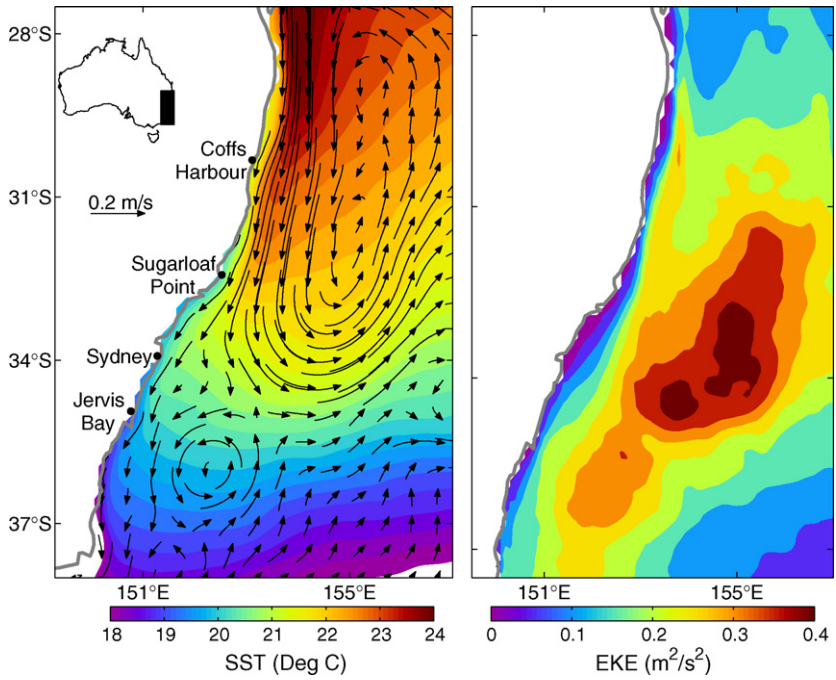

Fig. 1. Thirteen-year average SST and surface velocities (left) and EKE (right) from BRAN2.1. The inset on the left panel shows the location of the region of interest off south eastern Australia.

makes the initialisation of an ocean forecast in this region difficult and sometimes unreliable. It is expected that the assimilation of new additional observation types, like those planned under IMOS, will improve the forecast skill of the Bluelink system in the Tasman Sea. In this paper, the likely benefits to the Bluelink system of assimilating shelf observation platforms, including high-frequency (HF) land-based radar arrays (Lipa and Barrick, 1983) and gliders (Sherman et al., 2001; Webb et al., 2001), are assessed. In this study, the glider transects are treated in a way that is equivalent to repeat ship-borne conductivity–temperature–depth sections – and could equally be regarded as such. The assimilation of observations from gliders is described by Shulman et al. (2009) and the benefits of assimilating observations from HF radars into coastal ocean models has been well documented (Lewis et al., 1998; Oke et al., 2002; Shulman et al., 2002; Paduan and Shulman, 2004).

There are many examples of the use of data assimilation tools to influence the design of observing networks. These include the design of: mooring arrays in the tropical oceans (Hackert et al., 1998; Ballabrera-Poy et al., 2007; Oke and Schiller, 2007a; Vecchi and Harrison, 2007; Sakov and Oke, 2008); criteria of the Argo program (Guinehut et al., 2002; Schiller et al., 2004) and; monitoring strategies for the North Atlantic meridional overturning circulation (Hirschi et al., 2003; Baehr et al., 2004; Baehr et al., 2008). Other studies have examined the relative importance of different components of the GOOS for constraining a data assimilating ocean model (e.g., Oke and Schiller, 2007b). There are many examples from the numerical weather prediction community where data assimilation tools are used for array design and adaptive sampling (Bishop et al., 2003, 2006). This includes the international program, The Observing System Research and Predictability EXperiment (THORPEX; Rabier et al., 2007). Similarly, there are examples in the oceanographic community where modelling and data assimilating models have been used to guide adaptive sampling (Wilkin et al., 2005) including the Adaptive Sampling And Prediction (ASAP) program (www.princeton.edu/∼dcsl/asap/). The use of models and data assimilation tools to aid the design of observing systems is gaining acceptance in the oceanographic community.

This manuscript has three main objectives. The first is to describe and evaluate an ensemble-based method for assessing the current GOOS; and the second is to assess the likely benefits of assimilating new shelf observations into the Bluelink system; and the third is to explore the relative merit of different options for the deployment of new observation platforms. The calculations presented in this study use error estimates from the Bluelink system that is described in Section 2. The method for observing system assessment and design is presented in Section 3; and the results are presented in Section 4. A discussion is presented in Section 5 along with a summary in Section 6.

2. Bluelink reanalysis system

To familiarise the reader, an overview of the Bluelink system is provided, along with a description of the error estimates used therein and an example of results from a recent Bluelink reanalysis.

The Bluelink project was established to develop the first Australian operational short-range forecast system of the mesoscale ocean circulation around Australia. As a consequence, the data assimilation system (BODAS) used in Bluelink and in this study is not optimal, but it is comparable to other operational systems used around the world. The Bluelink system uses OFAM (Schiller et al., 2008), a global configuration of the Modular Ocean Model (Griffies et al., 2004), with 1/10° resolution around Australia and 10 m resolution down to 200 m depth.

The data assimilation system used under Bluelink is BODAS (Oke et al., 2008). BODAS employs an ensemble optimal interpolation (EnOI) scheme that uses a stationary, 120-member ensemble of intraseasonal model anomalies to approximate the system's background error covariance. When developing BODAS, it was anticipated that the background field (BGF) errors in BRAN would be dominated by errors in the locations and characteristics of eddies; and would therefore look like anomalies associated with eddies, but with shorter length-scales. The statistics of the ensemble, referred to above, are intended to quantify the BGF errors and their covariance. Each ensemble member is therefore generated by subtracting a three day mean from a seasonal climatology—both of which are derived from a model run with no data assimilation. This yields ensemble members that contain anomalies like those associated with an eddy field. Ideally, the anomalies contained in the ensemble should represent possible error fields for the Bluelink model. The Bluelink ensemble is constructed in a manner

that retains much of the mesoscale variability. This is because we don not believe that, without data assimilation, the Bluelink model, or any model for that matter, is unlikely to be skilful at reproducing eddy dynamics, such as eddy generation, instability and evolution.

One ensemble member is generated from every month of the last 10 years of a 14-year model run that is forced with 6-hourly surface fluxes provided by the European Center for Medium Range Weather Forecasting. The covariance of the ensemble is used to approximate the background error covariance.

One of the benefits of using an ensemble-based assimilation system is that it readily admits multivariate covariances. This means that observations of one type, say sea-level anomaly (SLA), are used to update fields of all types—SLA, temperature (T), salinity (S), and the zonal and meridional components of velocity (u and v, respectively). The multivariate nature of ensemble data assimilation comes through the ensemble-based covariances. If two state elements vary together in the ensemble, then an observation of one will lead to an update to the other. Because EnOI uses a stationary ensemble of model anomalies to represent the background error covariances, as described above, these covariances are almost certainly inaccurate—they are an approximation, based on some hypothesis about the nature of the errors. The degree of success of the EnOI system depends on how well the stationary ensemble approximates the true, but unknown, background error covariances.

An important feature of BODAS is covariance localisation. Using ensemble data assimilation, the influence of an observation on the model state is determined by the ensemble-based covariance between the observed state element and all other state elements. Because the ensemble is small compared to the dimension of the model subspace, the ensemble is both rank-deficient and suffers from sampling error (Houtekamer and Mitchell, 2001; Mitchell et al., 2002; Oke et al., 2007). Sampling error may lead to long-distance covariances that are non-zero, but unrealistic. These long-distance covariances are eliminated by multiplying the ensemble-based covariance by a localising correlation function (Houtekamer and Mitchell, 2001). Here, the localising function is a homogeneous, isotropic, Gaussian function with an e-folding length-scale of 2.25°. As a result, the influence of an individual observation on the model state depends on both the ensemble-based covariances and the distance between the observed location and the location of each model state element. The details of the ensemble-based covariance, including the length-scales, inhomogeneity and the anisotropy, is retained when localisation is used. Rather the localisation provides an upper limit for the ensemble-based covariance. It retains the covariance structure around each observation location, but artificially reduces the distant covariances to zero smoothly according to the localising function.

To provide some degree of confidence in the ensemble used here (and by Bluelink) a sample of the latest BRAN experiment is presented, followed by a more rigorous assessment of the error estimates used for Bluelink in Section 4. A comprehensive assessment of a recent BRAN experiment, BRAN1p5, is presented by Oke et al. (2008). For example, Oke et al. (2008) show that BRAN fields in the region around Australia are typically within 6–12 cm of withheld altimetric observations, within 0.5–0.9° of observed SST and within 4–7 cm of observed coastal sea-level. Comparisons with Argo profiles and surface drifting buoys show that BRAN fields are within 1° of observed sub-surface temperature, within 0.15 psu of observed sub-surface salinity and within 0.2 m s^{-1} of near-surface currents.

For the latest BRAN experiment, BRAN2p1 (Schiller et al., 2008), OFAM is updated by BODAS sequentially, once a week, by assimilating observations that include along-track SLA from altimeters, in situ T and S from Argo and other sources, and sea-surface temperature (SST) from the AMSR-E mission and Pathfinder database. The details of the assimilation are described by Oke et al. (2008). A series of comparisons between 6-day composite AVHRR SST fields and 5-day averaged SST from BRAN is shown in Fig. 2. Overlaid on the BRAN SST fields are 5-day Lagrangian trajectories, derived from the time-varying surface velocities computed by BRAN. Note that BRAN does not assimilate the high-resolution SST data shown in Fig. 2, rather it assimilates spatially averaged fields of AMSR-E SST, with nominal spacings of 0.5–1.0°. These comparisons highlight the energetic nature of the circulation in the Tasman Sea, particularly in the region south of 32°S, where EAC eddies frequently develop. BRAN shows good agreement with the observed features, demonstrating that BRAN can realistically represent the time-varying mesoscale circulation in the Tasman Sea (Fig. 2). This demonstrates that the EnOI system, including the error estimates therein, while not optimal, is capable of constraining an eddy-resolving model in this highly energetic region. These comparisons are drawn from a period when BRAN performs quite well. There are other periods when the eddy field is not as well reproduced by BRAN.

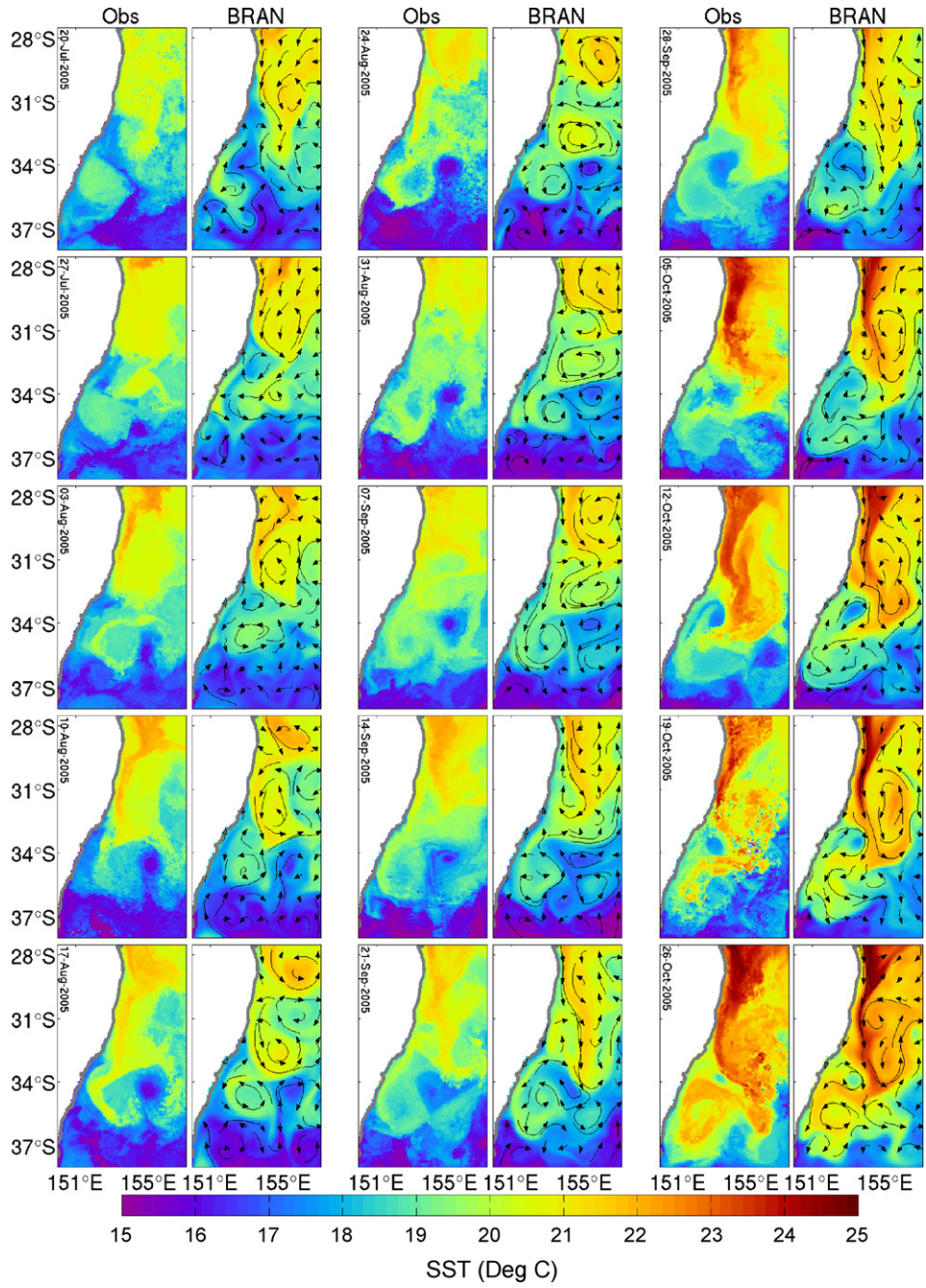

Fig. 2. A series of comparisons between 6-day composite AVHRR SST (columns 1, 3 and 5) and 5-day averaged SST from BRAN2p1 with 5-day Lagrangian trajectories from reanalysed surface velocities overlaid (columns 2, 4 and 6).

3. Method

3.1. Estimation of analysis errors

Data assimilation theory is used to assess the observing system and its design (e.g., Miller and Cane, 1989; Evensen, 2003). A brief description of the relevant components of this method is included here.

Suppose we have a discrete system that is characterised by a state vector $x^{n\times 1}$, and let us assume that the uncertainty of x is characterised by a background error covariance matrix P^{b}. The diagonals of P^{b} are the background error variance of each state element; representing the errors of the BGF before observations are assimilated. After assimilating a set of observations the uncertainty of the analysed system is characterised by the analysis error covariance matrix P^{a}. The diagonals of P^{a} are the analysis error variance of each state element; representing the errors of the analysis after observations are assimilated. According to Kalman Filter theory (e.g., Miller and Cane, 1989), P^{a} is given by

$$P^{\mathrm{a}} = [I - P^{\mathrm{b}}H^{\mathrm{T}}(HP^{\mathrm{b}}H^{\mathrm{T}} + R)^{-1}H]P^{\mathrm{b}}, \tag{1}$$

where I is the identity matrix; the superscript T denotes a matrix transpose; R is the observation error covariance matrix and H is an operator that interpolates from the model grid to observation locations. In all the scenarios considered in this paper, we assume that the observation errors are uncorrelated; that is, that R is diagonal. Given some estimate of P^{b}, Eq. (1) provides us with a means of estimating the expected analysis error variance of different observing systems by simply modifying H and R. For example, to estimate the theoretical analysis error for the GOOS H is defined so that it represents observations from altimeters, satellite SST and in situ platforms, like Argo; R is defined to represent the expected observation errors of each observation; and finally P^{a} is computed using (1) and its diagonals are used to quantify the theoretical analysis error variance. The accuracy of the theoretical analysis errors from (1) depends on the accuracy of the observation operator H and the estimated BGF and observation errors (P^{b} and R).

The dimension of the matrices P^{b} and P^{a} is $n \times n$, where n is the dimension of the state vector n that includes all model variables at all model grid points. These matrices can be very large, making their manipulation and storage practically impossible.

3.2. Ensemble-based approach to the estimation of analysis errors

Instead of explicitly storing and manipulating P^{b}, one may store and manipulate the covariance matrix implicitly via a representative ensemble A^{b} of the system state anomalies, $A^{b}_{n\times m} = [\delta x_{(1)}, \ldots, \delta x_{(m)}]$, where $\delta x_{(i)}$ is the ith model anomaly that is intended to represent a possible sample of the system error and m is the ensemble size. For Bluelink, a 120-member ensemble of intraseasonal model anomalies is used, as described in Section 2. The background error covariance P^{b} associated with the ensemble A^{b} is given by

$$P^{\mathrm{b}} = \frac{1}{m-1}A^{\mathrm{b}}A^{\mathrm{bT}}, \tag{2}$$

assuming that the ensemble mean of A^{b} is zero.

Using this ensemble-based approach to the estimation of P^{b}, given a set of observation types of known error (quantified by R) and known locations (quantified by H), we can readily update the background ensemble $A^{\mathrm{b}} \rightarrow A^{\mathrm{a}}$ in such a way that the covariance of A^{a}, calculated by

$$P^{\mathrm{a}} = \frac{1}{m-1}A^{\mathrm{a}}A^{\mathrm{aT}}, \tag{3}$$

matches the theoretical analysis error covariance given by (1). There are a number of formally equivalent solutions for the ensemble update, $A^{\mathrm{b}} \rightarrow A^{\mathrm{a}}$, that are associated with ensemble square root filters (Tippett et al., 2003). For the calculations presented in this study, the ensemble is updated using the ensemble implementation of the Potter algorithm, described by Whitaker and Hamill (2002), because it readily permits the use of covariance localisation. Briefly, the ensemble is updated for one observation

Table 1
Estimated observation error variances used for the diagonals of R for different observation types.

Observation platform	Variable	Estimated observation error variance
Altimeter	SLA	8^2 cm^2
AMSR-E SST	SST	0.25^2 K^2
HF radar	Surface velocity, (u, v)	0.1^2 [m s^{-1}]^2
Glider	Temperature, T	0.25^2 K^2
Glider	Salinity, S	0.05^2 psu^2

at a time using

$$A^{\mathrm{a}} = A^{\mathrm{b}} - \alpha KHA^{\mathrm{b}}, \tag{4}$$

where α is given by

$$\alpha = \left(1 + \sqrt{\frac{R}{HPH^{\mathrm{T}} + R}}\right)^{-1}, \tag{5}$$

and

$$K = r \circ PH^{\mathrm{T}}(HPH^{\mathrm{T}} + R)^{-1}. \tag{6}$$

Here, R and HPH^{T} are scalars, r is the localising correlation function and $r \circ P$ denotes an element by element multiplication, following Houtekamer and Mitchell (2001). For this study, an isotropic, homogeneous Gaussian correlation function is used, with an e-folding scale of 2.25°—the same as that used by BODAS for BRAN (Section 2).

Localisation in (6) is an ad-hoc modification to the Kalman filter. It is not represented in the theory used to derive (1). But localisation is included here, and in most ensemble data assimilation systems, to reduce sampling error of the ensemble-based covariances in (2); and to increase the effective rank of the ensemble A^{b} (Houtekamer and Mitchell, 2001; Mitchell et al., 2002; Oke et al., 2007). When using localisation in (6), the impact of a given observation is explicitly limited spatially. Close to an observation, the impact is virtually unmodified, but its influence gradually reduces to zero for distant elements. Another impact of including localisation in (6) is that the variance of A^{a} will always be greater than that without localisation. As the localising length-scale increases, the variance of A^{a} approaches that of the diagonals of P^{a} from (1).

The theory described above allows us to address two important goals of this study. Firstly, using information about the GOOS and error estimates used by BODAS (2)–(6) can be used to calculate the theoretical analysis error variance of fields produced using BODAS. The information about the GOOS required includes the type of variables observed (SLA, SST, T and S) and their spatial locations (altimeter tracks, satellite swaths and Argo locations), quantified by H, and their errors, quantified by R. By comparing the theoretical analysis errors to the actual errors, derived from a BRAN experiment, an evaluation can be made of the extent to which the theoretical errors match the actual errors. This provides an evaluation of both the method described here and the error estimates used in Bluelink. Secondly, R and H can be manipulated to represent new, hypothetical observations to obtain an estimate of the likely analysis errors achievable when new observation platforms are assimilated.

3.3. Observation error estimates

The calculations presented in this study include representation of observations of SLA along altimeter tracks, SST along satellite swaths, in situ T and S at locations of Argo profiles and along idealised glider transects and surface velocity (u and v) with idealised spatial footprints that represent short-range or long-range land-based HF radar arrays. Table 1 lists the estimated observation error variances used in R for different observation platforms. The estimated observation errors for SLA, SST and in situ T and S are based on those used in the latest BRAN experiments (Oke et al., 2008; Schiller et al., 2008) and are described in Section 2. The estimated observation error for surface velocity from HF

radar arrays are based on results presented by Ohlmann et al. (2007). Note that the estimated errors in Table 1 include contributions of the instrument error, associated with expected accuracy of each observation platform, representation error (e.g., Oke and Sakov, 2008), associated with sub-grid-scale variability, and an average age error, associated with the use of an observation window that spans several days. These observation errors are typically dominated by representation error, depending on the application. For a more detailed explanation of these error sources, the reader is referred to Oke et al. (2008). The observation errors estimated here are probably larger than one might expect. This reflects the combined error sources that are represented by R.

3.4. Statistics to quantify improvement

In Section 4, the expected improvement due to the assimilation of a set of observations is quantifies by computing the percentage improvement $\%I$, that is defined here as

$$\%I_{\mathrm{GOOS}} = \frac{\varepsilon^{\mathrm{BGF}} - \varepsilon^{\mathrm{An}}_{\mathrm{GOOS}}}{\varepsilon^{\mathrm{BGF}}} \times 100, \tag{7}$$

$$\%I_{\mathrm{GOOS+New}} = \frac{(\varepsilon^{\mathrm{An}}_{\mathrm{GOOS}} - \varepsilon^{\mathrm{An}}_{\mathrm{GOOS+New}})}{\varepsilon^{\mathrm{An}}_{\mathrm{GOOS}}} \times 100, \tag{8}$$

where $\%I_{\mathrm{GOOS}}$ is the $\%I$ of adding the GOOS relative to the BGF and $\%I_{\mathrm{GOOS+New}}$ is the %I of adding the New observations, relative to assimilation of observations from the GOOS; $\varepsilon^{\mathrm{BGF}}$ is the estimated standard deviation of the BGF error; $\varepsilon^{\mathrm{An}}_{\mathrm{GOOS}}$ is the standard deviation of the analysis error using observations from the GOOS and $\varepsilon^{\mathrm{An}}_{\mathrm{GOOS+New}}$ is the standard deviation of the analysis error using observations from the GOOS and observations from the new observation platform. If the addition of a new platform has no impact on the analysis error, $\varepsilon^{\mathrm{An}}_{\mathrm{GOOS+New}}$ will be equal to $\varepsilon^{\mathrm{An}}_{\mathrm{GOOS}}$ and $\%I_{\mathrm{GOOS}}$ from (8) will be zero. If the addition of a new platform reduces the analysis error to zero, $\%I_{\mathrm{GOOS}}$ from (8) will be 100%. Each error estimate in (7) and (8) is calculated from the standard deviation of A^{b} or A^{a} that are described above. The new platforms considered here include surface velocity from HF radar and in situ T and S from gliders.

Recall that one of the objectives of this study is to assess the relative merit of, for example, one glider transect compared to another. We assess this by comparing the $\%I$ expected for different options. This is the motivation for using this metric. We do not necessarily anticipate any meaningful certain structure to the $\%I$, but we hope that the structure of the theoretical $\%I$ is similar to the structure of the actual $\%I$, so that our results are meaningful for comparing different options for the shelf observing system.

4. Results

In this section, the validity of the Bluelink error estimates and the method (Sections 2 and 3) are assessed, by comparing the theoretical errors to the actual errors of the Bluelink system. The analysis errors and $\%I$ are subsequently estimated for different observing systems, including different options for HF radar arrays and glider transects.

4.1. Evaluation of the method and error estimates using only the GOOS

To evaluate the Bluelink error estimates and the method, described in Sections 2 and 3, the estimated and theoretical errors to the actual errors for both SLA and SST are compared (Figs. 3 and 4). Specifically, the estimated BGF errors are compared to the actual BGF errors from the latest BRAN experiment (panels a and b). Similarly, the theoretical analysis errors are compared to the actual analysis errors from the latest BRAN experiment (panels c and d). Note that the range of BGF and analysis errors are an order of magnitude different. The theoretical and actual $\%I$, from (7), is also presented in Figs. 3 and 4 (panels e and f).

The estimated BGF errors (panel a in Figs. 3 and 4) are the square root of the diagonals of P^{b}, from (2), using the ensemble employed by the Bluelink system as input. This estimate is stationary—and does not depend on the details of any observing system.

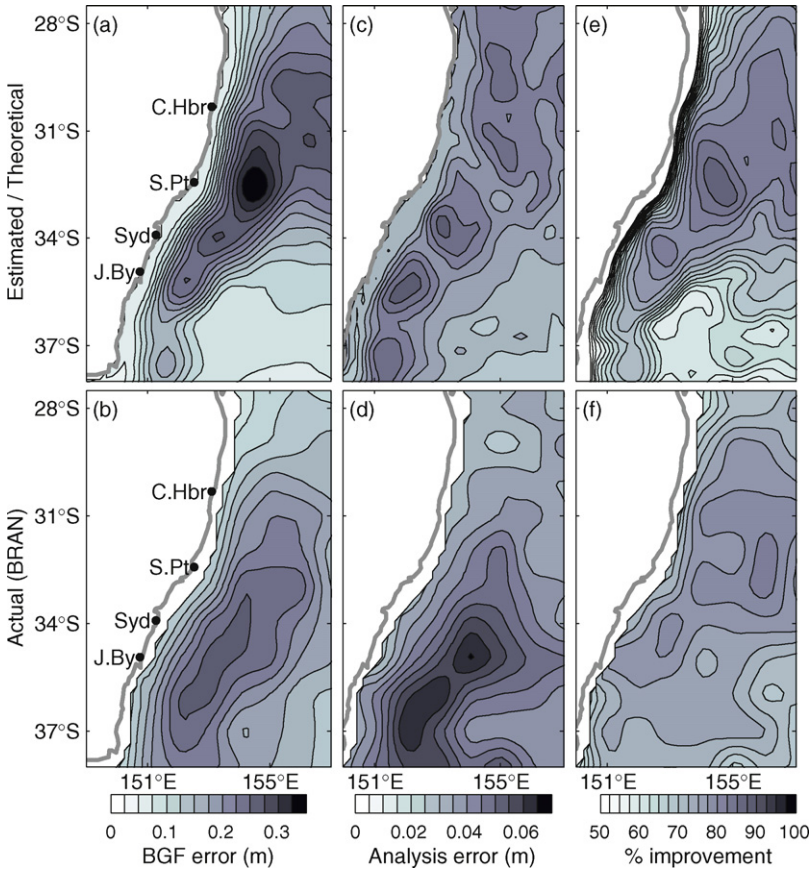

Fig. 3. Maps showing the estimated and theoretical (top) and actual (bottom) BGF errors (a and b), analysis errors (c and d) and percentage improvement (e and f), from (7), for SLA. Contour intervals for the BGF error, analysis error and %*I* are 0.03 m, 0.005 m and 2.5% respectively. Note that the range is different for the BGF and analysis errors.

The theoretical analysis errors (panel c in Figs. 3 and 4) are the square root of the diagonals of (3), using (4)–(6) to transform $A^{b} \rightarrow A^{a}$, given H and R that represent the observations assimilated into BRAN. The details of the theoretical analysis errors are particularly sensitive to the locations of observations, represented by H. Because the spatial distribution of both satellite and in situ observations in the GOOS varies considerably over time, any single estimate of A^{a} may not be representative of the time-mean analysis errors. Two examples of the theoretical analysis error for SLA, computed using observations from the GOOS for consecutive weeks at the start of 2005, are shown in Fig. 5. Note that the SLA and SST locations correspond to the locations of super-observations—that are spatially averaged from altimeter tracks and satellite swaths respectively. Super-observations are routinely used in Bluelink to reduce the computational cost of the assimilation system (Oke et al., 2008). In these examples there are localised regions with relatively large error where there are fewer SLA observations from the GOOS (e.g., 156°E, 32°S, panel b). To eliminate this sampling error, 52 different versions of A^{a} are computed, one for each week of 2005, using the real distribution of SLA, SST and in situ T and S observations from the real GOOS for each week. This yields 52 estimates of the theoretical analysis error, based on 52 different but realistic, realisations of the GOOS. These estimates are subsequently averaged to produce the fields in Figs. 3c and 4c.

The actual BGF and analysis errors (panels b and d in Figs. 3 and 4) are computed from the latest BRAN experiment (BRAN2p1; Schiller et al., 2008). Specifically, the actual errors are calculated using

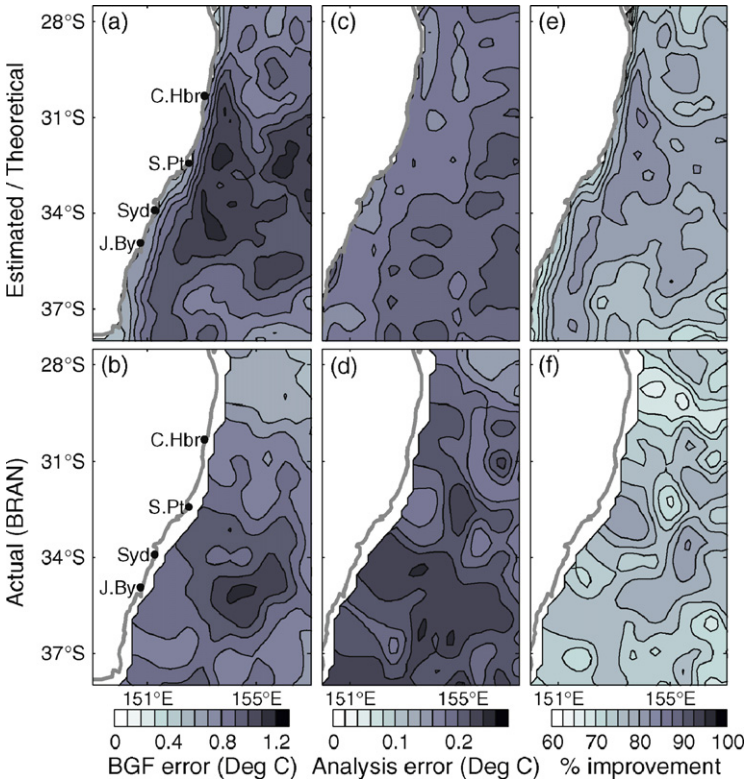

Fig. 4. As for Fig. 3, except for SST. Contour intervals for the BGF error, analysis error and %*I* are 0.1°, 0.02° and 2.5% respectively. Note that the range is different for the BGF and analysis errors.

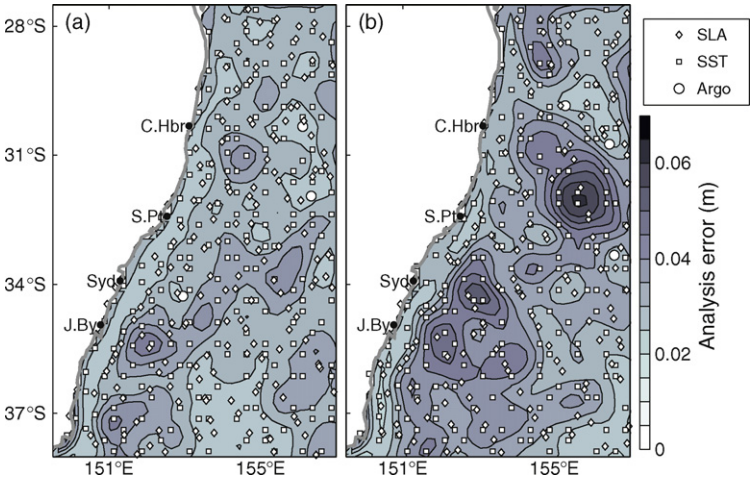

Fig. 5. Examples of the theoretical analysis error for SLA for two examples (a and b), one week apart, computed using different samples of the GOOS observations. Contour intervals are 0.005 m. Note that SLA observations are not restricted to altimeter tracks because they are spatially averaged prior to assimilation (see Oke et al., 2008, for details).

the statistics of the BGF and analysis innovations (differences from observations) for a 3-year period spanning January 2004 to December 2006. These innovations are binned into 1 degree boxes in the Tasman Sea. The standard deviation of the error in each bin is computed and interpolated to the model grid. The error estimates for SLA are produced by using innovations for SLA along altimeter tracks (Fig. 3). Similarly, the error estimates for SST are produced by using the innovations for AMSR-E SST (Fig. 4). To obtain the estimates of error in BRAN, presented in Figs. 3 and 4, the SLA and SST observations are implicitly regarded as error-free (i.e., any deviation from the observations and BRAN is regarded as an error in BRAN). This is, of course, in conflict with the assumption that observations contain error, as described in Section 3 and summarised in Table 1. However, in the absence of an alternative method for estimating the actual errors in BRAN, we proceed with this approach.

The estimated BGF errors and the theoretical analysis errors for SLA (Fig. 3a and c) are different to the actual BGF and the actual analysis errors respectively (Fig. 3b and d). This demonstrates that there is an inconsistency in the error estimates used under Bluelink. That is, the error estimates used for Bluelink themselves, contain error—they are an approximation to the true, but unknown, errors, as prefaced in Section 2. However, there are similarities between these fields. All of these error maps show a ridge of relatively high error oriented parallel to the coastline, with lower errors near the shelf and to the south-east corner of the region shown. The magnitudes of the theoretical and actual errors are in reasonably agreement. For example, along the ridge of maximum error, the BGF errors for SLA are 0.25–0.35 m (Fig. 3a and b) and the analysis errors are 0.05–0.07 m (Fig. 3c and d) for both the theoretical and actual error estimates. The estimated BGF error shows the maximum error between 31°S and 33°S, where the EAC typically separates from the coast. By contrast, the actual BGF error has a maximum between 33°S and 37°S, where the EAC eddy field is typically very energetic and often quite confused (e.g., Fig. 2). This indicates that while the Bluelink system does a better job than expected at representing the EAC variability near the separation point (expected—meaning implicitly in the ensemble), it apparently does a worse job than expected at evolving the eddy field. The latter point is probably attributable to errors introduced by initialisation that are not explicitly represented in the ensemble. Initialisation is the artificial shock that results when a model is restarted with a dynamically unbalanced field. This shock typically degrades the forecast, causing the BGF errors to increase.

Despite the differences between the estimated and actual BGF errors and the theoretical and actual analysis errors for SLA (Fig. 3) the percentage improvement, calculated using (7), is similar for both the theoretical errors and the actual errors (Fig. 3e–f). This is important for this study, because this metric is used for most of the analysis presented in the remainder of this paper. Both the theoretical and actual percentage improvement have similar spatial patterns, with relatively large values around 32–33°S and smaller values around the boundaries of the domain shown here. The anomaly correlation for the two estimates of percentage improvement is 0.84, the RMS difference is 10.5% and the bias is −5.4%, with the actual improvement slightly less than the theoretical estimate.

The theoretical and actual errors for SST are shown in Fig. 4. Again, the estimated BGF errors and the theoretical analysis errors for SST (Fig. 4a and c) are different to the actual errors estimated for BRAN (Fig. 4b and d). Similarly, the theoretical and actual percentage improvement is different for SST (Fig. 4e and f), however note that these fields are quite noisy with less coherent structure than the corresponding fields for SLA. The magnitude of the theoretical and actual errors are again quite consistent. South of about 32°S, for example, both the theoretical and actual BGF errors for SST are between 0.8 and 1.2 °C that reduces to around 0.2–0.3 °C through the process of assimilation. Similarly, the percentage improvement is of the same order for both the theoretical and actual fields—both indicate a reduction in the error through assimilation of between 70 and 85%. The anomaly correlation between the theoretical and actual percentage improvement is 0.38, the RMS difference is 5.5% and the bias is 3.6%, with the theoretical improvement slightly larger than the actual improvement.

The comparisons in Figs. 3 and 4 assess the validity of both the error estimates used under Bluelink and the methodology described in Section 3. For both SLA and SST, the theoretical and actual errors show some similarities and some differences. For both variables, the percentage improvements show some agreement between the theoretical and actual fields. The key question for this study is whether these error estimates are useful for assessing new, hypothetical observation types. Stated another way, with reference to Figs. 3 and 4, suppose panels a, c and e in each figure are produced prior to integrating BRAN, using them to predict the likely errors in BRAN. In hindsight, would these estimates be a useful

first guess of the actual errors? If the answer this is positive, then the following analysis used to assess new observation platforms will be useful.

4.2. Assessment of new observation platforms

Before investigating the impact of adding a new shelf observation platform to the GOOS, the estimated BGF errors and the theoretical analysis errors are presented for different variables when observations from the GOOS are assimilated (Fig. 6). The variables considered here include u and v at the surface, T and S at the surface and at 205 m depth, and sea-level. When new observations are added to the GOOS, the magnitude of their estimated observation errors (Table 1) relative to the analysis errors using the GOOS (Fig. 6) become important. Effectively, prior to the assimilation of observations from a new platform, the BGF errors are equivalent to the analysis errors when observations from the GOOS are assimilated (Fig. 6). For example, the theoretical analysis error for surface velocity, when observations from the GOOS are assimilated, are 0.15–0.2 m s^{-1} within 100 km or so of the coast (top two rows of Fig. 6). This includes the regions where the HF radar observations may be made. It is assumed that the HF radar observations have an error of 0.1 m s^{-1} (Table 1). The assumed observation error is less than the theoretical analysis error using the GOOS—so we might expect the HF radar observations to have a significant impact on surface velocity when the radar is added to the GOOS. By contrast, the magnitude of the assumed T and S observations from glider observations (Table 1) are comparable to the magnitude of the theoretical analysis errors using the GOOS for SST and sea-surface salinity (SSS), respectively (rows 3 and 5 of Fig. 6). We might therefore expect the addition of the glider observations to the GOOS to only yield moderate reduction in the analysis errors for SST and SSS, although this would clearly not be the purpose of deploying gliders.

To evaluate the potential impact of new observation platforms on the Bluelink system, the percentage improvement, using (8), is calculated for several variables for cases with different hypothetical HF radar arrays in Fig. 7. This quantifies the improvement to the analysis error attributable to the addition of the new observation platform. That is, given observations from the GOOS, the %I gained by also assimilating observations from the new shelf platform is quantified. As described above, for all of these calculations 52 different estimates of the theoretical analysis error are computed using realistic

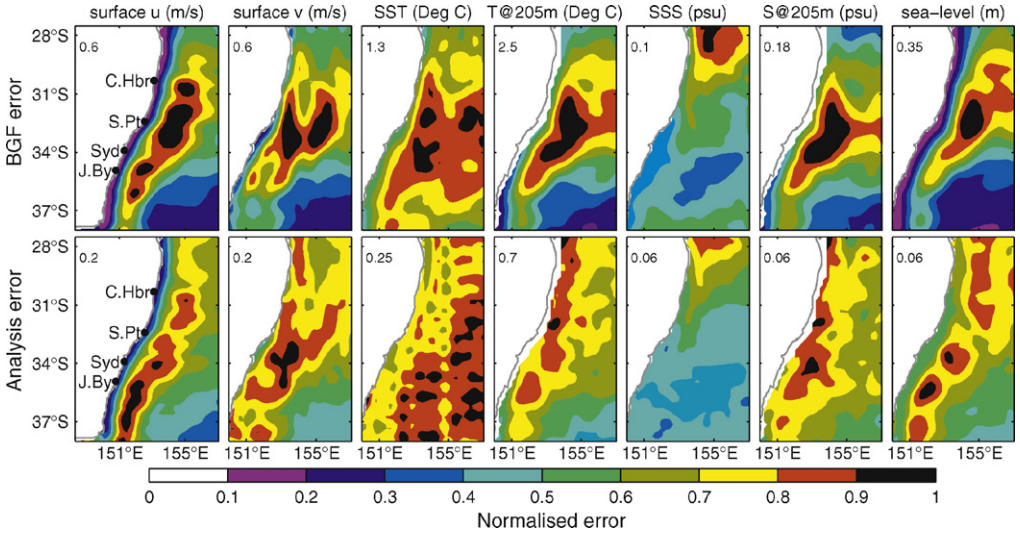

Fig. 6. Estimates of the BGF error (top) and the analysis error when observations from the GOOS are assimilated (bottom), for variables surface u and v, SST, T at 205 m depth, SSS, S at 205 m depth and sea-level (left-right). The legend shows the normalised error. Each panel is normalised by the number shown in the top left corner of each panel.

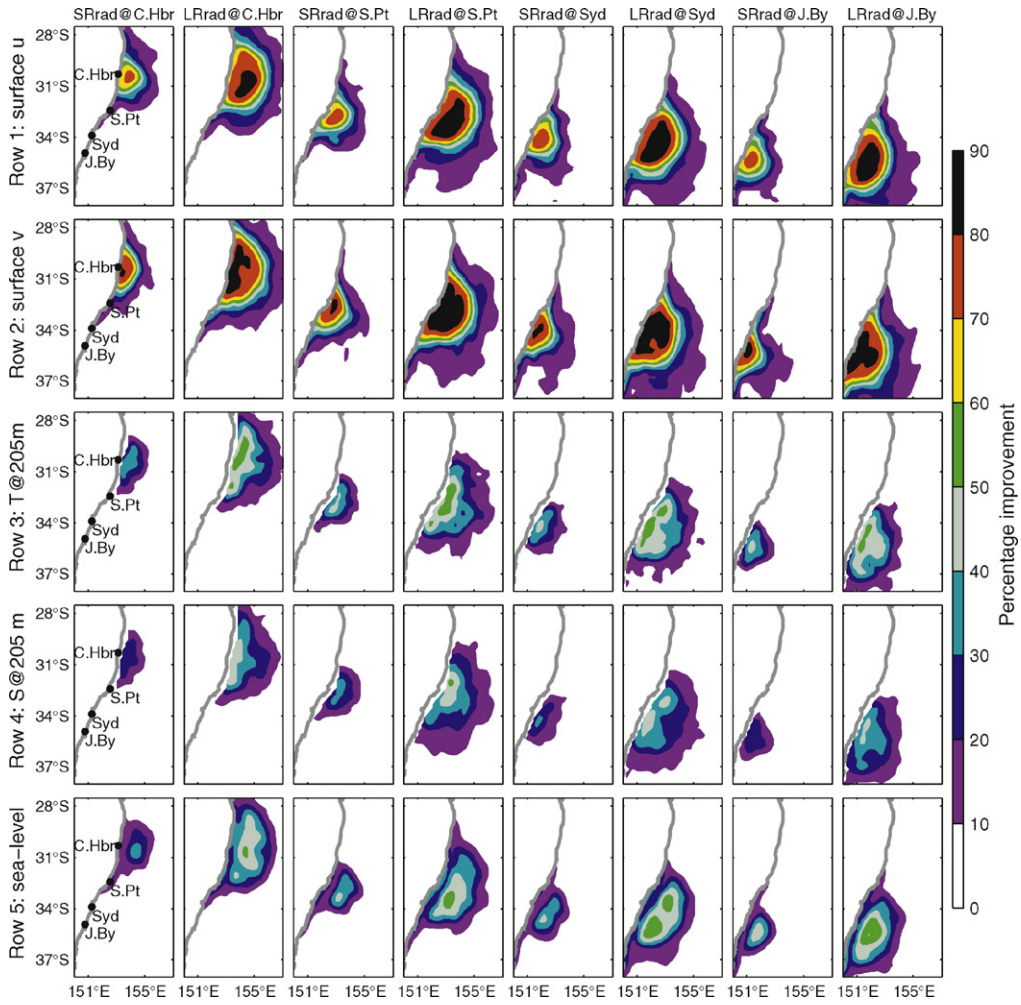

Fig. 7. Estimates of the percentage improvement, from (8), for the u and v (row 1–2); for T and S at 205 m depth and sea-level (row 5) for short-range (SRrad) and long-range (LRrad) HF radar arrays (assumed to observe surface velocity) off Coffs Harbour (C.Hbr, column 1–2), Sugarloaf Point (S.Pt, columns 3–4), Sydney (Syd, columns 4–5) and Jervis Bay (J.By, columns 7–8). The locations of the u and v observations are indicated in each column by the gray dots.

distributions of observations from the GOOS, plus observations from the new, hypothetical observation platform that are assumed to be fixed in space and time. These 52 estimates of the theoretical analysis error and $\%I$ are subsequently averaged.

The HF radar options considered in Fig. 7 includes both short-range and long-range radars off Coffs Harbour (30.3°S), Sugarloaf Point (32.5°S), Sydney (34°S) and Jervis Bay (35.1°S) using the observation error estimates presented in Table 1. It is assumed that the short-range and long-range radars have a range of 100 km and 200 km respectively and that they measure surface velocity at a horizontal resolution of 20 km (the HF radar observations will be sub-sampled, or spatially averaged to 20 km prior to assimilation). For each case considered here the surface velocity fields are well constrained by the HF radars, with improvements of up to 80% for the regions that are directly sampled. The region of influence extends beyond the observed region for all cases, with significant improvements to the analysis errors for u and v up to 200 km beyond the observed region. The multivariate features of EnOI are shown here in the percentage improvements to variables that are not directly observed by the HF

radars. Analysis errors for sea-level and sub-surface T and S decrease by up to 60% in some regions by the long-range radar and by up to 30–40% for short-range radars.

Interestingly, sea-level is better represented by the radars that are farther to the south (Fig. 7). The case involving a long-range radar off Jervis Bay, for example, indicates a significant improvement in sea-level in the observed region. This is a region that is not always well constrained by the Bluelink system using the GOOS (Fig. 3b and d). Perhaps the altimeter tracks are too coarse to adequately sample the small-scale, energetic circulation in this region. In this case, it appears that a long-range radar off Jervis Bay may go some way towards filling this gap in the GOOS.

The theoretical analysis error for sub-surface T and S show the greatest improvement over the shelf and slope, rather than offshore (Fig. 7). This can be seen by the strip of 50–60% improvement for the long-range radar aligned with the coast. This may be because the HF radar will likely monitor variations in the strength and position of the EAC that is known to drive current-driven upwellings (Oke and Middleton, 2001). These current-driven upwellings are likely to be represented here by correlations between sub-surface T and S over the shelf and slope with surface velocity.

The percentage improvement, using (8), is also presented for some idealised glider transects along the coast in Fig. 8. In each case, a glider is assumed to travel at a constant latitude between the coast and 200 km offshore. Moreover, T and S observations are assumed to have been processed into vertical profiles every 20 km along the transect. The improvement to sub-surface T and S is quite localised in each case. The analysis errors for T and S is reduced significantly immediately along the glider path, but this improvement drops off quite quickly to the north, south and offshore. This localised drop off in the percentage improvement is on much shorter spatial scales than the localising function used in (6). This indicates that the decorrelation length-scales between T and S along the coast are quite short. These short length-scales in the ensemble are confirmed in Fig. 9, showing the localised ensemble-based correlations between T at 205 m depth at a reference location and T at 205 m depth in the surrounding region. These fields demonstrate the region of influence of an observation at the reference location. Where the magnitude of these correlations are high, the influence of a T observation from that location is significant. The examples shown in Fig. 9 include correlations when the reference location is on the continental shelf, the continental slope and over the deep ocean, where the bottom depth is 105, 775 and 3600 m respectively. These reference locations are spaced 0.5° apart. The length-scales are clearly shorter near the coast and increase offshore. In each case, the correlation fields show a ridge of relatively high correlation along a south-east to north-west axis, roughly corresponding to the direction of a separating EAC. The results shown in Figs. 8 and 9 indicate that if a network of gliders were to be deployed along the entire NSW coast, the spatial separation of the glider transects along shore would have to be relatively small (probably around 100 km) if the entire shelf is to be represented.

The percentage improvement to surface v is up to 50% for the regions shown here (second row of Fig. 8). The improvement to u, is less than that of v, but is still significant and displays some interesting spatial patterns (top row of Fig. 8). It tends to show a greater improvement to the north and south of each transect, compared to along the transect. This is probably due to the dominance of geostrophy in the ensemble statistics. Also, there tends to be greater improvement to the north of each transect, relative to the south. THis is probably because the circulation to the north tends to be more organised. When a localised update is applied to the density field along a shore-normal section (like the glider transects) the reduction in the magnitude of this update to the north and south (evident in rows 3 and 4 of Fig. 8) manifests itself as an adjustment to the meridional density gradient. The geostrophic adjustment to such a density gradient, represented here through the ensemble statistics, would involve a meridional flow with a sign that depends on the nature of the gradient. As a result, the percentage improvement for u is small along the observed transect, where the horizontal gradient of the density update (attributable to the glider observations) is small, and somewhat larger to the north and south, where the horizontal gradient of the density update is likely to be largest.

The improvement to sea-level due to gliders varies for different transects along the coast (Fig. 8). Off the north and south coast of NSW the improvements to sea-level are similar to that of sub-surface T and S. However, off central NSW at 32°S, where the EAC typically separates from the coast, the improvement to sea-level is less. This is because the relationships between T, S and sea-level are weaker here, owing to the complex nature of the circulation at this location.

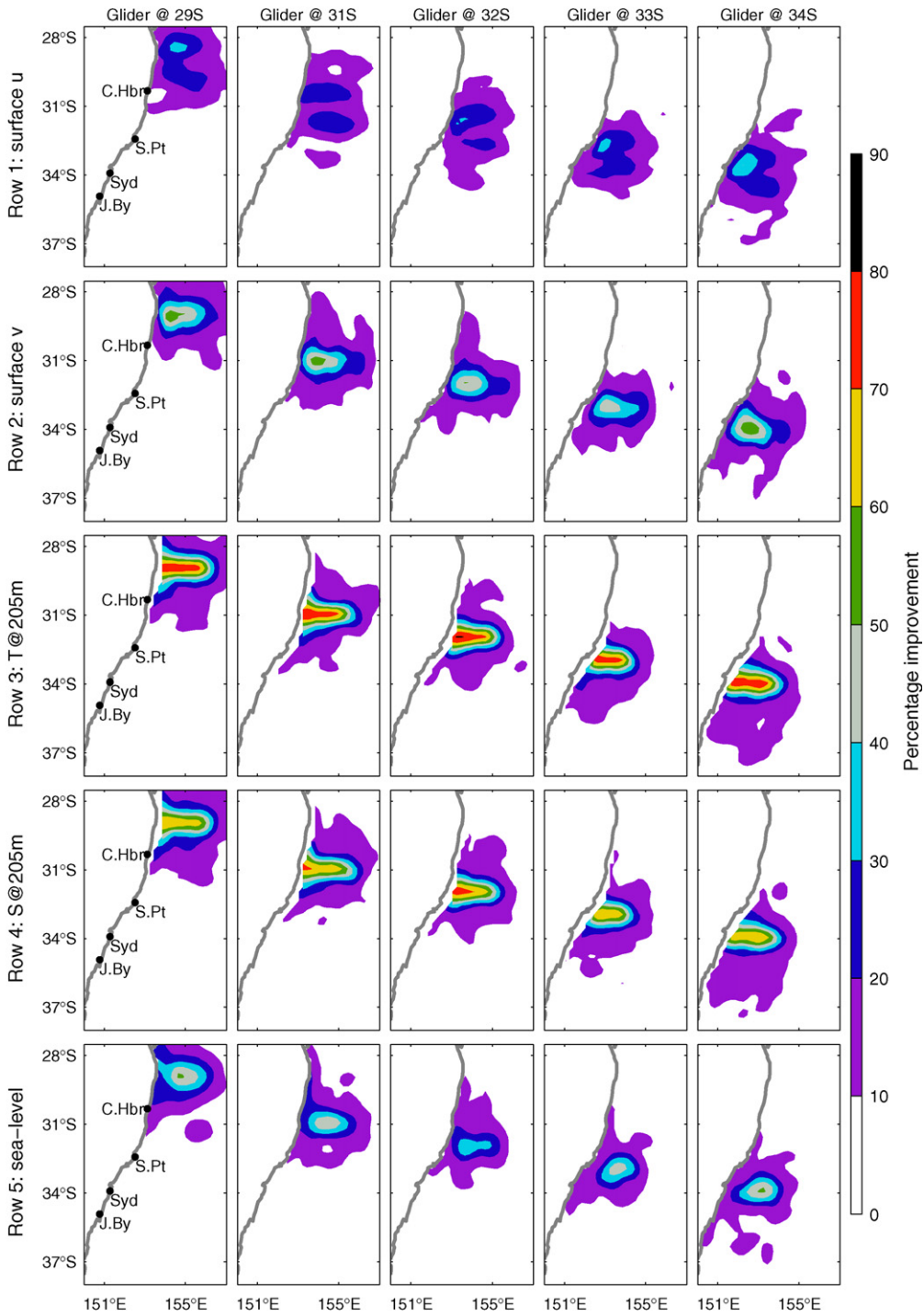

Fig. 8. As for Fig. 7, except for repeat glider transects at different latitudes. The locations of the *T* and *S* observations are indicated in each column by the black dots.

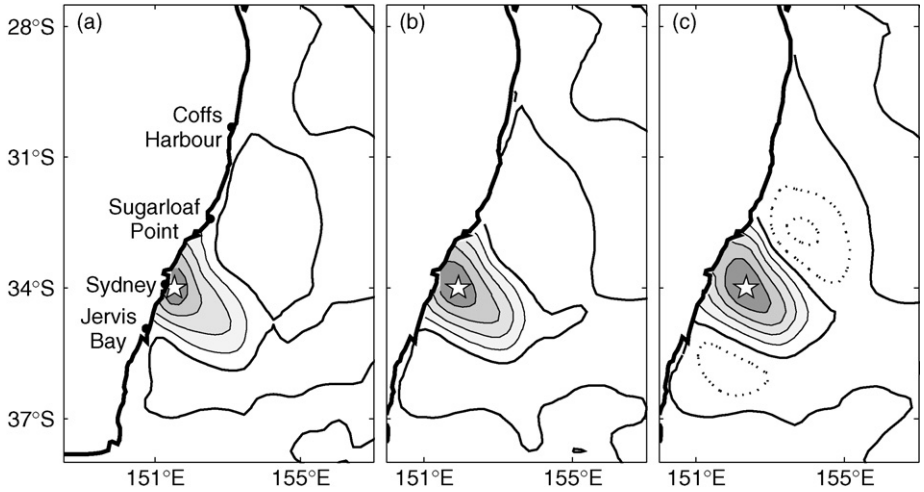

Fig. 9. Examples of the ensemble-based cross-correlation between T at 205 m depth at the reference location, denoted by the star, and T at 205 m depth in the surrounding region for a reference location (a) on the continental shelf, (b) over the continental slope and (c) over the deep ocean at 33°S off eastern Australia. Contour intervals are 0.2; zero is bold, dotted is negative, correlations above 0.6 are shaded.

To concisely compare different shelf observation platforms for assimilation into the Bluelink model, evaluation regions are defined around each platform's measurement locations. For each new platform an evaluation region that is within one e-folding scale (using the same localising length-scale used in (6)) of at least one observation made by that platform is defined. Some examples of these regions are shown in Fig. 10. This is intended to make the influence of localisation in the assimilation approximately the same for each platform. The theoretical analysis errors and percentage improvement are simply averaged for each variable and for each new platform over these evaluation regions. The results are displayed in Fig. 11, showing the area-averaged error estimates and the percentage improvements respectively.

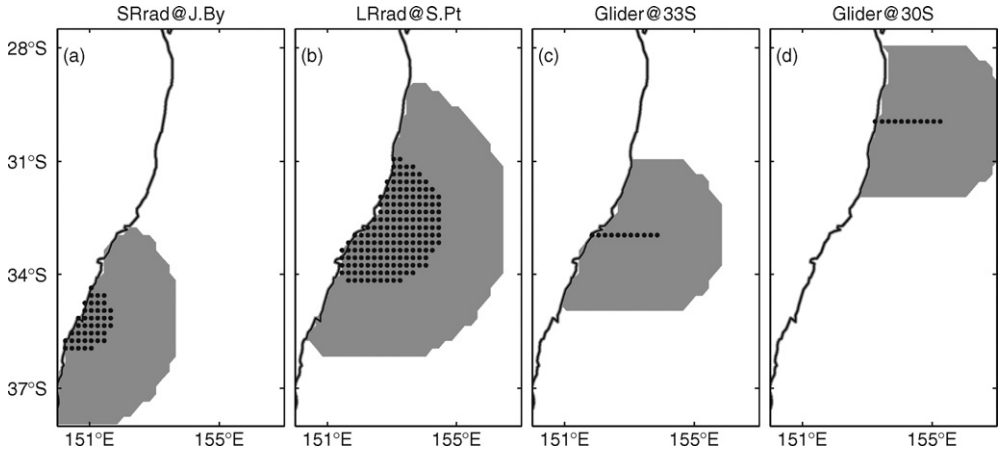

Fig. 10. Evaluation regions for selected new observational platforms. The grey area denotes the evaluation region and the black dots denote the assumed observation locations. In each case the observation region is within one e-folding length-scale of at least one observation location.

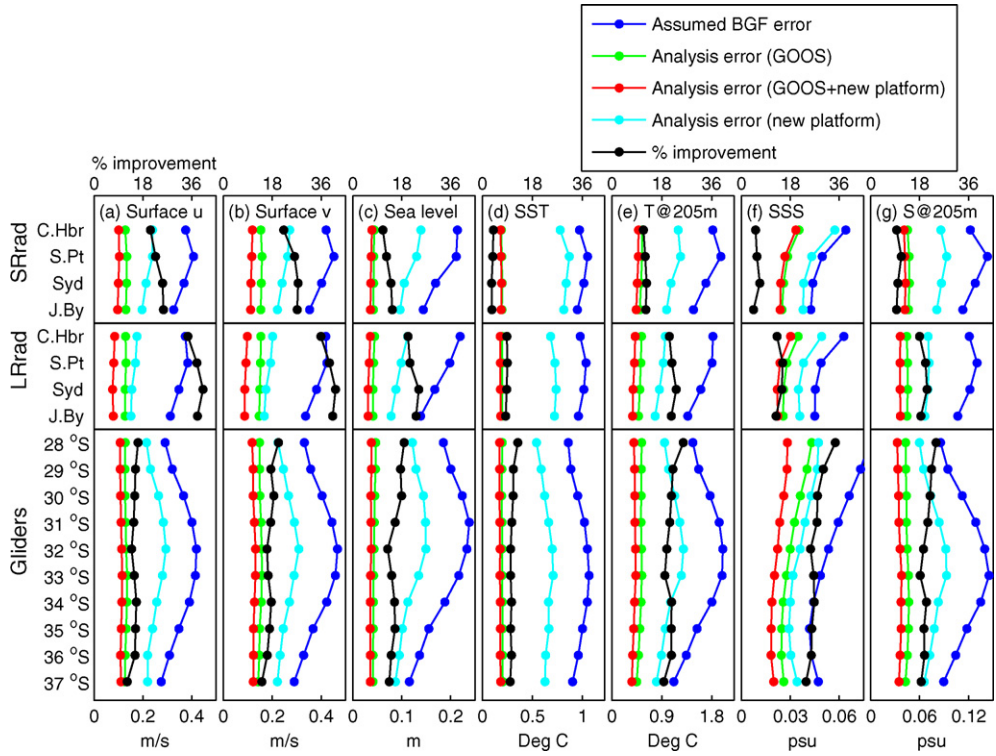

Fig. 11. The estimated BGF error, calculated analysis errors and % improvement, from (8), for different combinations of the GOOS and each new platform, averaged over the corresponding evaluation region (see Fig. 10), for different variables (left-to-right). Results for short-range HF radar are the top 4 points, long-range HF radar are the next 4 points and gliders are the bottom 10 rows, as labelled. The scale for % improvement is above each panel.

The area-averaged errors for the BGF, the analysis errors using only the GOOS, the analysis errors using both the GOOS and the new observation platform, and the analysis error using only the new observation platform. The difference between the analysis error using the GOOS and the analysis errors using both the GOOS and the new platform provides an indication of "how much" the new observation platform adds to the GOOS. The difference between the BGF error and the analysis error using only the new platform provides an indication of how much the new observation platform may improve the Bluelink system in the absence of the GOOS. Overall, the results indicate that a new observation platform, either HF radar or glider, will probably add a modest amount of skill to the forecast and reanalysis system as long as observations from the GOOS are assimilated, and provided the GOOS coverage does not degrade.

It is clear that the long-range radars are likely to provide a better return to the Bluelink system than the short-range radars (Fig. 11). This is expected, given the significantly larger footprint of the long-range systems. However, in practice, the spatial resolution of the short-range radars is higher than the long-range radars and may therefore be more useful for understanding and monitoring small-scale shelf processes, though this is not assessed in this study.

Fig. 11 includes the percentage improvement, computed using (8), when each new observation platform is added to the GOOS. For example, consider the $\%I$ for surface u when long-range HF radar is deployed off Coff Harbour. In this case, the analysis errors in surface u decrease by around 35% in the evaluation region. Based on the statistics in Fig. 11, it appears that gliders along the northern NSW coast are likely to be slightly more beneficial for constraining T and S than those to the south. However,

this difference is marginal and probably not significant given the uncertainties in the evaluated errors, as evident in Figs. 3 and 4.

The impact of HF radar observations on sub-surface T and S is surprisingly high (Fig. 11e and g)—around 20% improvement. One might have assumed that the sub-surface T/S variability would be in the null space of the surface u/v variability. Apparently, the covariances in the ensemble used here include significant covariance between surface u/v and sub-surface T/S. This is presumably due to the dynamical coupling of these variables in the model from which the ensemble is derived. Moreover, the % improvement in sub-surface T/S is similar for both glider and HF radar assimilation. This is likely to be due to the difference in the number of observations assimilated from these different platforms and the broader foot-print of the HF radar observations.

Clearly, none of the shelf observation platforms are likely to have a significant impact on the analysis errors for SST (Fig. 11). This is probably because the analysis errors for SST using the GOOS alone (Figs. 4 and 6) are small, and are comparable to the magnitude of the observation errors for the T observations from gliders (Table 1).

5. Discussion

There are many aspects of the design and assessment of observing systems that are not addressed in this study. The glider program, for example, may be intended to accurately monitor various characteristics of the EAC, like the transport along a shore-normal transect. The observed transport across the current is likely to be an accurate snapshot of the oceanic conditions that can be used to ultimately understand variability over many different time-scales. An assessment of the shelf observations for these purposes has not been attempted here. Instead, the scope of this study is limited to understanding the impacts of assimilating new observation platforms on the Bluelink system. Other limitations of this study include the unrealistic assumptions that gliders can be deployed along predetermined paths and that HF radars can be deployed anywhere along the coast. In practice, these points depend on a range of different factors that are not addressed here. However, as noted in the introduction, the treatment of glider transects in this study is equivalent to repeat ship-borne conductivity–temperature–depth sections, with profiles every 20 km across the shelf. It is also also assumed that there are no data gaps in the observations and, for simplicity, the impact of glider-based velocity estimates are not included in our assessment of gliders.

In Section 4, it is found that the gliders are likely to have only a modest impact on the analysis errors of the system. This is because the variables measured by the gliders (T and S) are also represented (though not directly) by observations from the GOOS. So even without the gliders the observations from the GOOS have reduced the errors of the mapped fields to values that are comparable to the assumed observation error of the gliders (Fig. 6). The impact of the gliders depends on both the assumed observation error (Table 1) and the ensemble-based covariances (Fig. 9). As discussed in Section 3, the observation error is dominated by the representation error. The error estimates for representation error used here are conservative (i.e., larger than one might expect). This is consistent with the general approach for the Bluelink system (Oke et al., 2008). We would rather under-utilise observations than over-fit them. Over-fitting can be bad. The worst case scenario for over-fitting is that it causes the model to become numerically unstable. There's a subtlety regarding representation error. From an assimilation perspective, the representation error of an observation depends on the resolution of the model into which we are assimilating (Oke and Sakov, 2008). If glider observations were to be assimilated, for example, into a very high resolution model, the model should be able to represent all of the features measured by the glider—so the representation error would be close to zero. By contrast, if glider observations were assimilated into a coarse resolution model, the model would not be able to represent all of the features observed by the glider (eddies for example), so the representation error is large—roughly as large as the signals associated with the features that the model cannot resolve. The Bluelink system sits somewhere in the middle, resolving scales of around 50 km and greater. So, although the gliders might be quite accurate (with small instrument error), the Bluelink system would not be able to take full advantage of their accuracy because it cannot resolve all of the observed scales properly. As a result of this, the analysis in the paper underestimates the true (scientific) value of the observations, but are a true assessment from the perspective of using these data to constrain the Bluelink model.

As noted in Section 2, the success of EnOI and the relevance of the study presented here depends on the degree to which the estimated background error covariances are correct. In practice, the background error covariances are unknown and so must be approximated. In this study, we assess the ensemble-based covariances used here and under Bluelink in two ways. Firstly, we present a series of qualitative comparisons between reanalysed and with-held SST fields in Fig. 2. Through these comparisons we show that BRAN can realistically reproduce the mesoscale ocean circulation. Since the performance of BRAN implicitly depends on the background error covariances used by the assimilation, we argue that the estimated ensemble-based covariances are reasonable. This is a necessary, but not sufficient condition, for the ensemble-based estimates to be regarded as true. Secondly, we attempt an explicit comparison of the estimated/theoretical background and analysis error variances and the actual background and analysis error variances in Figs. 3 and 4. These comparisons involve the estimation and comparison of errors. Due to the absence of complete knowledge of the true fields, these errors are unknown, and are approximated. The approximations that under-pin these comparisons and based on several assumptions. Despite these uncertainties, we argue that the general agreement between the estimated/theoretical errors and the actual errors – their relative magnitudes, for example – justifies the use of these error estimates for the purpose of guiding the assessment and design of observing systems. The assessment presented here is clearly not the complete story. Many other aspects of the circulation, the implementation and maintenance of instruments, and the intended use of the observations must also be considered. However, we argue that the type of analysis performed here will help build intuition and provide some guidance when the design of observing systems is undertaken.

This study is motivated by the IMOS program. Under IMOS, a specific design for the NSW node has been proposed (www.imos.org.au/nswimos.html). This includes the deployment of a HF radar off Coffs Harbour, gliders off Sydney, moorings along the NSW coast as well as other observation platforms. We have not attempted to remain true to the details of the NSW-IMOS proposal in this study. For example, the glider program off Sydney is intending to adaptively direct gliders to specific oceanographic features, like cold-core eddies, rather than occupy the same transect repeatedly over a sustained period. Instead, we have tried to examine various options that are possible under IMOS that we think might add value to the Bluelink project.

Throughout this paper, the focus is on the impact of different observations on analysis errors. By contrast, Oke and Schiller (2007b) assess the impact of existing components of the GOOS on the forecast skill of a model. They achieve this through a series of observing system experiments, where each component of the GOOS is systematically with-held from the assimilation. In practice, the interpretation of an assessment of impacts on forecast skill is more complicated than an assessment of impacts on analysis errors. This is because forecast skill not only depends on the magnitude of analysis errors, but also on factors such as initialisation (e.g., Oke et al., 2008). Initialisation refers to the process where the model adjusts to introduced dynamical imbalances after it is initialised, often resulting in a deterioration of the subsequent forecast. By focusing only on analysis errors here, this complication has been avoided. However, a consequence of focussing on analysis errors is that the dynamical forward interpolation of information by the model has not been included. For example, suppose a glider is deployed along the northern NSW shelf. This may improve the ocean state at that location and subsequently improve the forecast to the south, downstream, as this information is advected by the EAC. Similarly, suppose a glider is deployed along the southern NSW shelf. This may improve the ocean state at that location and subsequently improve the forecast to the north, as this information is propagated northwards by coastal trapped waves. The model's response to the reduction in analysis error has not thoroughly been assessed here. This means that our analysis has not addressed the likely impacts of gliders, for example, on improving aspects of the forecast like heat, freshwater and volume transports.

6. Summary

A simple, computationally efficient method that quantifies the likely impact of observations on the analysis error of an EnOI-based data assimilation system is described. This method is used to explore the likely benefits of assimilating observations from shelf observation platforms, including HF radars

and gliders that may be deployed in the future. The method exploits various aspects of ensemble data assimilation theory. Our investigations are directly relevant to the Bluelink system that runs operationally at the Bureau of Meteorology to produce short-range forecasts of the mesoscale ocean circulation around Australia. The Bluelink system is also routinely used for ocean reanalyses. Results from a multi-year reanalysis are used to estimate the actual BGF and analysis errors of SLA and SST; and compare these observations to theoretical estimates obtained using the above-mentioned method. This provides an evaluation of both the error estimates used under Bluelink and the described method. While the results demonstrate an inconsistency in the Bluelink error estimates, there are enough similarities in the actual and theoretical error estimates to provide a useful first approximation to the likely benefits of future observation platforms.

The likely improvements to the Bluelink system are assessed when observations of surface velocity from HF radar arrays are assimilated; and when in situ T and S observations are assimilated from hypothetical glider transects. The results suggest that, provided the Bluelink system continues to assimilate observations from the GOOS, namely altimetry, SST and Argo, and provided the GOOS coverage does no degrade, we should expect only a modest reduction to analysis errors of some variables, but quite a significant reduction to others.

The assimilation of surface velocities from long-range HF radar would likely reduce analysis errors in surface velocity by up to 80%; and that the improvement to surface velocity may not be confined to the region that is directly observed, but that it may extend up to 200 km beyond the HF radar footprint. Also, the results indicate that the analysis errors for SLA may be significantly reduced by long-range HF radar assimilation, particularly off the NSW south coast. This is probably because short length-scale processes, like cold-core eddies, are not always well resolved by the GOOS, but should be well-resolved by a HF radar array. In this case the deployment of a long-range HF radar array may effectively fill a gap in the GOOS in some locations.

The experiments in this study suggest that neither HF radar or glider observations are likely to improve SST significantly. In part, this is because the GOOS does a good job of observing SST already. However, the results indicate that the assimilation of HF radar or glider observations may have a significant positive impact on sub-surface T and S, and SSS in the vicinity of the observations. This is because of the relatively sparse observations of sub-surface T and S and the lack of SSS observations. The calculations imply that the impact of glider observations are likely to be quite localised, around the transects that are directly observed. This to attributed to the short decorrelation length-scales of T and S over the shelf. This means that if a glider program was to be established, to monitor T and S using the Bluelink system to map the observations, the glider transects may need to be quite closely spaced (probably around 100 km) in order to properly resolve the mesoscale variability over the shelf.

The conclusions drawn in this study about different observation platforms off NSW are based on an assessment of their likely impact on the Bluelink forecast and reanalysis system. We reiterate that the observing systems proposed under IMOS have not been designed with the exclusive requirements of Bluelink in mind. We therefore expect that the assessments presented in this study, while important to the future developments and planning of ocean forecast and reanalysis systems like Bluelink, are likely to under-estimate the scientific value of the observations from other perspectives, like that described above.

In this study the utility of ensemble data assimilation systems is demonstrated. While the design and assessment of an observing system using data assimilation tools is sensitive to the details of that system (e.g., error variance and covariance estimates), many more general results become evident, like length-scales, multivariate relationships and even the capacity of current observing systems. These results help build intuition about the observational requirements to properly monitor the ocean and we expect the continued use of models and data assimilation to aid the design of observing systems to become a standard and important step in this process.

Acknowledgments

Financial support for this research is provided by the US Office of Naval Research and by CSIRO, the Bureau of Meteorology and the Royal Australian Navy as part of the Bluelink project. The authors

acknowledge M. Baird, G. Meyers and B. Sloyan for discussions that led to improvements in this manuscript.

References

Baehr, J., Hirschi, J., Beismann, J.-O., Marotzke, J., 2004. Monitoring the meridional overturning circulation in the North Atlantic: a model-based array design study. J. Mar. Syst. 62, 283–312.
Baehr, J., McInerney, D., Keller, K., Marotzke, J., 2008. Optimization of an observing system design for the North Atlantic meridional overturning circulation. J. Atmos. Oceanic Tech. 25, 625–634.
Ballabrera-Poy, J., Hackert, E., Murtugudde, R., Busalacchi, A.J., 2007. An observing system simulation experiment for an optimal moored instrument array in the tropical Indian Ocean. J. Climate 20, 3284–3299.
Bishop, C.H., Reynolds, C.A., Tippett, M.K., 2003. Optimization of the fixed global observing network in a simple model. J. Atmos. Sci. 60, 1471–1489.
Bishop, C.H., Etherton, B.J., Majumdar, S.J., 2006. Verification region selection and data assimilation for adaptive sampling. Q. J. R. Meteor. Soc. 132, 915–933.
Evensen, G., 2003. The ensemble Kalman filter: theoretical formulation and practical implementation. Ocean Dyn. 53, 343–367.
Griffies, S.M., Pacanowski, R.C., Rosati, A., 2004, A technical guide to MOM4. GFDL Ocean Group Technical Report No. 5. NOAA/Geophysical Fluid Dynamics Laboratory, 371 pp.
Guinehut, S., Larnicol, G., Le Traon, P.-Y., 2002. Design of an array of profiling floats in the North Atlantic from model simulations. J. Mar. Syst. 35, 1–9.
Hackert, E.C., Miller, R.N., Busalacchi, A.J., 1998. An optimized design for a moored instrument array in the tropical Atlantic Ocean. J. Geophys. Res. 103, 7491–7509.
Hirschi, J., Baehr, J., Marotzke, J., Stark, J., Cunningham, S., Beismann, J.-O., 2003. A monitoring design for the Atlantic meridional overturning circulation. Geophys. Res. Lett. 30, 1413, doi:10.1029/2002GL016776.
Houtekamer, P.L., Mitchell, H.L., 2001. A sequential ensemble Kalman filter for atmospheric data assimilation. Mon. Wea. Rev. 129, 123–137.
Lewis, J.K., Schulman, I., Blumberg, A.F., 1998. Assimilation of doppler radar current data into numerical ocean models. Cont. Shelf Res. 18, 541–559.
Lipa, B.J., Barrick, D.E., 1983. Least-squares methods for the extraction of surface currents from CODAR cross-looped data: Application at ARSLOE. IEEE J. Oceanic Eng. OE-8, 226–253.
Miller, R.N., Cane, M.A., 1989. A Kalman filter analysis of sea level height in the tropical Pacific. J. Phys. Oceanogr. 19, 773–790.
Mitchell, H.L., Houtekamer, P.L., Pellern, G., 2002. Ensemble size, balance, and model-error representation in an ensemble Kalman filter. Mon. Wea. Rev. 130, 2791–2808.
Ohlmann, C., White, P., Washburn, L., Terrill, E., Emery, B., Otero, M., 2007. Interpretation of coastal HF radar-derived surface currents with high-resolution drifter data. J. Atmos. Oceanic Technol. 24, 666–680.
Oke, P.R., Middleton, J.H., 2001. Nutrient enrichment off Port Stephens: the role of the East Australian Current. Cont. Shelf Res. 21, 587–606.
Oke, P.R., Allen, J.S., Miller, R.N., Egbert, G.D., Michael Kosro, P., 2002. Assimilation of surface velocity data into a primitive equation coastal ocean model. J. Geophys. Res. 107, 3122–3147.
Oke, P.R., Schiller, A., Griffin, D.A., Brassington, G.B., 2005. Ensemble data assimilation for an eddy-resolving ocean model of the Australian Region. Q. J. R. Met. Soc. 131, 3301–3311.
Oke, P.R., Sakov, P., Corney, S.P., 2007. Impacts of localisation in the EnKF and EnOI: experiments with a small model. Ocean Dyn. 57, 32–45.
Oke, P.R., Schiller, A., 2007a. A model-based assessment and design of a tropical Indian ocean mooring array. J. Climate 20, 3269–3281.
Oke, P.R., Schiller, A., 2007b. Impact of Argo SST and altimeter data on an eddy-resolving ocean reanalysis. Geophys. Res. Lett. 34, L19601, doi:10.1029/2007GL031549.
Oke, P.R., Brassington, G.B., Griffin, D.A., Schiller, A., 2008. The Bluelink Ocean Data Assimilation System (BODAS). Ocean Mod. 21, 46–70, doi:10.1016/j.ocemod.2007.11.002.
Oke, P.R., Sakov, P., 2008. Representation error of oceanic observations for data assimilation. J. Ocean. Atmos. Technol. 25, 1004–1017.
Paduan, J.D., Shulman, I., 2004. HF radar data assimilation in the Monterey Bay area. J. Geophys. Res. 109, doi:10.1029/2003JC001949.
Rabier, F., Gauthier, P., Langland, R., 2007. Objectives of the THORPEX working group on data assimilation and observing strategies for high impact weather forecast improvements. Geophys. Res. Abs. 9, 04024.
Sakov, P., Oke, P.R., 2008. Objective array design: application to the tropical Indian Ocean. J. Atmos. Oceanic Technol. 25, 794–807.
Schiller, A., Wijffels, S.E., Meyers, G.A., 2004. Design requirements for an Argo float array in the Indian Ocean inferred from observing system simulation experiments. J. Atmos. Ocean. Technol. 21, 1598–1620.
Schiller, A., Oke, P.R., Brassington, G.B., Entel, M., Fiedler, R., Griffin, D.A., Mansbridge, J., 2008. Eddy-resolving ocean circulation in the Asian-Australian region inferred from an ocean reanalysis effort. Prog. Oceanogr. 76, 334–365.
Sherman, J., Davis, R.E., Owens, W.B., Valdes, J., 2001. The autonomous underwater glider 'Spray'. IEEE J. Oceanic Eng. 26, 437–446.
Shulman, I., Wu, C.R., Lewis, J.K., Paduan, J.C., Rosenfeld, L.K., Kindle, J.C., Ramp, S.R., Collins, C.A., 2002. High resolution modeling and data assimilation in the Monterey Bay area. Cont. Shelf Res. 22, 1129–1151.
Shulman, I., Rowley, C., Anderson, S., DeRada, S., Kindle, J., Martin, P., Doyle, J., Cummings, J., Ramp, S., Chavez, F., Frantoni, D., Davis, R., 2009. Impact of glider data assimilation on the Monterey Bay Model. Deep Sea Res. 56, 188–198, doi:10.1016/j.dsr2.2008.08.003.
Tippett, M.K., Anderson, J.L., Bishop, C.H., Hamill, T.M., Whitaker, J.S., 2003. Ensemble square root filters. Mon. Wea. Rev. 131, 1485–1490.

Vecchi, G.A., Harrison, M.J., 2007. An observing system simulation experiment for the Indian Ocean. J. Climate 20, 3300–3343.
Webb, D.C., Simonetti, P.J., Jones, C.P., 2001. SLOCUM: an underwater glider propelled by environmental energy. IEEE J. Oceanic Eng. 26, 447–452.
Whitaker, J.S., Hamill, T.M., 2002. Ensemble data assimilatrion without perturbed observations. Mon. Wea. Rev. 130, 1913–1924.
Wilkin, J.L., Arango, H.G., Haidvogel, D.B., Lichtenwalner, C.S., Glenn, S.M., Hedstrom, K.S., 2005. A regional ocean modeling system for the long-term ecosystem observatory. J. Geophys. Res. 110, C06S91, doi:10.1029/2003JC002218.